https://doi.org/10.18321/ectj1492

Effect of Lanthanum Oxide on the Activity Ni-Co/Diatomite Catalysts in Dry Reforming of Methane

G.Y. Yergaziyeva[1]*, E. Kutelia[2], K. Dossumov[1], D. Gventsadze[2], N. Jalabadze[2], T. Dzigrashvili[2], L. Nadaraia[2], O. Tsurtsumia[2], M.M. Anissova[1], M.M. Mambetova[1], B. Eristavi[2], N. Khudaibergenov[1]

[1]Institute of Combustion Problems, 172, Bogenbay batyr str., Almaty, Kazakhstan
[2]Georgian Technical University, 7, Kostova str., Tbilisi, Georgia

Article info

Received:
8 July 2022

Received in revised form:
10 September 2022

Accepted:
25 October 2022

Keywords:
Catalysis, Dry reforming of methane, Diatomite, Modifying additive, Methane conversion, Syngas

Abstract

The effect of modifying additive (La_2O_3) on the activity of Ni-Co oxides was studied for the dry reforming of methane (DRM). The catalysts were prepared by impregnation of the granulated diatomite (D) and characterized by SEM, EDX, H_2-TPR, XRD, and AES. It is shown that the addition of 1.5 wt.% La_2O_3 into the Ni-Co/D composition leads to an increase in the activity of the catalyst, providing a methane conversion that is close under thermodynamic equilibrium conditions in the temperature range of 700–850 °C. The highest activity is achieved at T = 850 °C, the conversion of methane is 96%, and carbon dioxide is 92%. The addition of lanthanum oxide to the Ni-Co/D composition led to an increase in catalyst stability; after testing in the DRM reaction for 360 min, the deactivation coefficient for methane was 3.4%, and for carbon dioxide 2.5%. While significant deactivation is observed for Ni-Co/D, the deactivation coefficient for methane is 19%, and for carbon dioxide 36%. Many characterization results (SEM, H_2-TPR, and XRD) confirm that Ni-Co-La/D has abundant surface oxygen and the presence of spinel structures that contribute to the reactivity of CH_4 and CO_2, which positively affect its activity.

1. Introduction

Carbon dioxide (CO_2) is the main greenhouse gas that contributes significantly to global warming and climate change. The main sources of CO_2 emissions are human activities, agricultural activities, and some industrial processes. Many efforts are currently being made to control and use CO_2. The most promising process for using CO_2 is the dry reforming of methane, the interaction of CO_2 and CH_4 to produce synthesis gas [1]. Dry methane reforming (DRM) is an efficient way to convert greenhouse gases (CO_2 and CH_4) in the presence of a catalyst into syngas with an H_2/CO ratio suitable for methanol synthesis and the Fischer-Tropsch process [2].

Typical catalysts for DRM are noble metals and catalysts based on transition metal oxides (Ni, Co, etc.). The high price of precious metals limits their widespread use. Nickel-based catalysts are as active as noble-metal catalysts. Their main disadvantage is rapid deactivation due to carbon deposition. Therefore, many researchers have explored various approaches to minimize carbon formation on nickel catalysts. It has been shown that, for nickel catalysts, the addition of oxides of alkaline earth and/or rare earth metals reduces coke formation due to the formation of carbonates or oxycarbonates during the reaction [3–6]. It has been suggested that the addition of promoters with basic properties such as MgO, CaO, and La_2O_3 can improve both catalyst performance and coke resistance [7]. It was found in [8, 9] that the addition of La_2O_3 to a Ni-containing catalyst can increase the dispersion of Ni particles on supports and reduce the agglomeration of Ni particles during DRM. In addition, lanthanum oxide can adsorb and react with CO_2 to form $La_2O_2CO_3$ particles on the catalyst surface, which can accelerate the conversion of CH_x surface particles [10].

*Corresponding author.
E-mail: ergazieva_g@mail.ru

Catalysts based on Co oxides are less active in the DRM reaction, but more stable to coking than nickel catalysts [11–13].

The effect of lanthanum oxide on the activity of 10 wt.% Co/MA was studied in [14], where the catalyst promoted with lanthanum oxide not only showed higher activity in DRM, but also gave less deposited carbon compared to the unpromoted cobalt catalyst. The increase in the activity of the cobalt catalyst with the addition of lanthanum oxide is associated by the authors with a decrease in the size of Co_3O_4 crystallites, with an improvement in the reducibility of the catalyst and an increase in the basic character.

Research of DRM is being carried out on both monometallic Ni- and Co-containing and bimetallic Ni-Co catalysts [15–17]. Recently, much attention has been paid to bimetallic catalysts. Ni-Co containing bimetallic catalyst was considered in [18]. Bian et al. and others [18–20] highlight the good coking resistance and catalytic performance of Ni-Co catalysts compared to other bimetallic transition element catalysts. These properties were associated with the formation of an alloy between Ni and Co and their mutual stabilization. Ni, which is more active in the dissociation of methane, is deactivated due to coking. In the activation of carbon dioxide, Co is more active, which is deactivated by reoxidation. In the Ni-Co bimetallic catalyst, the flow of hydrogen from Ni to Co prevents its oxidation, and the high affinity of cobalt for oxygen promotes the oxidation of carbon and reduces coking [21].

Very little has been written in the literature about the effect of lanthanum as a promoter on the activity of a Ni-Co containing bimetallic catalyst in DRM. There are works where lanthanum oxide was investigated as a support for Ni-Co [22–24].

The authors of [22, 24] obtained bimetallic catalysts with Ni-Co alloy nanoparticles well dispersed on a La_2O_3 support by reducing perovskite precursors $LaCo_xNi_{1-x}O_3$. Ni-Co-containing bimetallic catalysts showed high activity in the DRM reaction. The authors attribute this activity to the formation of highly dispersed Ni^0-Co^0 particles on the $La_2O_2CO_3$ matrix, which prevents coke formation, despite the harsh reaction conditions.

In addition to lanthanum oxide, various compounds have been studied as supports for Ni-Co: Al_2O_3, SiO_2, MgO, zeolites, etc. [25].

To make the developed catalysts available for wide industrial use, efforts are being made to limit the cost of materials not only concerning the deposited metal active phase but also by considering inexpensive and widely available media. In the last few years, some natural minerals, such as clinoptilolite [26], and diatomite [27], have been used as supports for catalysts for the dry conversion of methane. Among various porous materials, diatomite is more attractive due to its highly porous structure, low density, and large specific surface area [27].

Diatomite is a type of biogenic siliceous sedimentary rock formed as a result of the deposition of unicellular aquatic algae, consisting of a significant number of diatoms of various shapes and sizes.

Karam Jabbour [27] used diatomaceous earth as a substrate for the deposition of 5 wt.% NiO. A monometallic catalyst containing 5 wt.% Ni/diatomite and 5 wt.% Ni/SiO_2 was prepared by the two-solution (cyclohexane/water) precipitation method. Compared to Ni/SiO_2, the 5 wt.% Ni/diatomite catalyst was relatively stable during catalytic measurements carried out at 650 °C for 12 h. In addition, carbon deposits with lower toxicity (easier removed by reactivation) were obtained on the 5 wt.% Ni/diatomite catalyst than those formed on Ni/SiO_2.

The purpose of this work is to study the effect of lanthanum oxide on the activity of Ni-Co/diatomite catalysts in the processes of DRM. For the synthesis of catalysts, the method of capillary impregnation was used. In addition, diatomite from the Georgia deposit was used for the first time for DRM. The abundant and available diatomite mines encourage the industry to use it, which is cheaper than Al_2O_3. Therefore, synthesizing a highly efficient and stable diatomaceous earth catalyst can significantly reduce costs.

2. Materials and methods

2.1. Preparation of catalysts

Diatomite from the Kisatibi deposit, Georgia, was used as a support for Ni-Co and Ni-Co-La. Diatomite is crushed in a mill, coarse powders are obtained with a grain dispersion in the range of ~100÷400 μm. The obtained coarse powders are further crushed in a vibrating mill for 40 min to a fine-grained powder with particle sizes in the range of ~100 nm ÷ 5 μm. Then the resulting powder is granulated by molding in mini-form granules of the same shape (cylindrical, Ø2.7 mm, h = 2.7 mm). Diatomite granules are calcined at atmospheric pressure at a rate of 2 °C/min up to 600 °C in the air with a holding time of 1 h. The catalysts were prepared by capillary impregnation of the support. In the beginning, the moisture capacity (water capacity) of diatomite (support) was determined; for this,

1 g of diatomite granules was weighed and dried at a temperature of 120 °C for 20 min. Distilled water was added dropwise to the dried diatomite granules at room temperature and atmospheric pressure until the granules were saturated, the moisture capacity of 1 g of diatomite was 1.1 ml of water.

Bioxide Ni-Co/D (oxide ratio $NiO\text{-}Co_3O_4$ = 1.5:1) and polyoxide Ni-Co-La/D (oxide ratio $NiO\text{-}Co_3O_4\text{-}La_2O_3$ = 2:1.3:1) catalysts were prepared by the methods of capillary impregnation of the Diatomite (D) granules with water solutions of a mixture of metal salts $(Ni(NO_3)_2 \cdot 6H_2O$ (technical standard 4055-70), $Co(NO_3)_2 \cdot 6H_2O$ (technical standard 4528-78) and $La(NO_3)_3 \cdot 6H_2O$ (technical standard 6-09-4676-83). Heat treatment of the catalysts was carried out in an air stream at 300 °C for 2 h and at 500 °C for 3 h, at a rate of 3 °C/min [28].

2.2. Testing of catalysts and analysis of reaction products

Testing the activity of the synthesized catalysts in the dry reforming of methane as carried out on a flow-type laboratory unit (Fig. 1) [28]. Before the DRM, the catalysts were pretreated with 15% H_2/Ar at a gas hourly space velocity (GHSV) of 1000 h^{-1} for 180 min at 500 °C.

The gases exiting the reactor during the performance tests were analyzed by gas chromatograph (GC-1000 LLC "Chromos" Russia) with thermal conductivity detector on two columns: molecular sieve CaA column for N_2, H_2, and O_2, and HP/Plot Q column for CH_4, CO_2, and CO detection.

Process conditions: 0.1 MPa, the temperature was set in the range of 600–850 °C, the ratio of methane: carbon dioxide 1:1, and the volume of catalyst in the reactor was 2 ml (1.2 g).

The conversion of the initial methane (X_{CH4}), carbon dioxide (X_{CO2}), the yields of hydrogen (Y_{H2}) and carbon monoxide (Y_{CO}), the ratio of hydrogen to CO (H_2/CO), the deactivation coefficient for methane (DE_{CH4}), the deactivation coefficient for carbon dioxide (DE_{CO2}) were calculated according to the following equations:

$$X_{CH_4}(\%) = \frac{C_{CH_{4in}} - C_{CH_{4out}}}{C_{CH_{4in}}} \times 100 \quad (1)$$

$$X_{CO_2}(\%) = \frac{C_{CO_{2in}} - C_{CO_{2out}}}{C_{CO_{2in}}} \times 100 \quad (2)$$

$$Y_{H_2}(\%) = \frac{C_{H_{2out}}}{2C_{CH_{4in}}} \times 100 \quad (3)$$

$$Y_{CO}(\%) = \frac{C_{COout}}{C_{CH_{4in}} + C_{CO_{2in}}} \times 100 \quad (4)$$

$$\frac{H_2}{CO} = \frac{C_{H2out}}{C_{CO_{out}}} \quad (5)$$

$$DE_{CH_4}(\%) = \frac{X_{CH_4}^{in} - X_{CH_4}^{out}}{X_{CH_4}^{in}} \times 100 \quad (6)$$

$$DE_{CO_2}(\%) = \frac{X_{CO_2}^{in} - X_{CO_2}^{out}}{X_{CO_2}^{in}} \times 100 \quad (7)$$

where X_i (in/out) is the initial conversion (in) and conversion after 360 min (out) of CH_4 and CO_2.

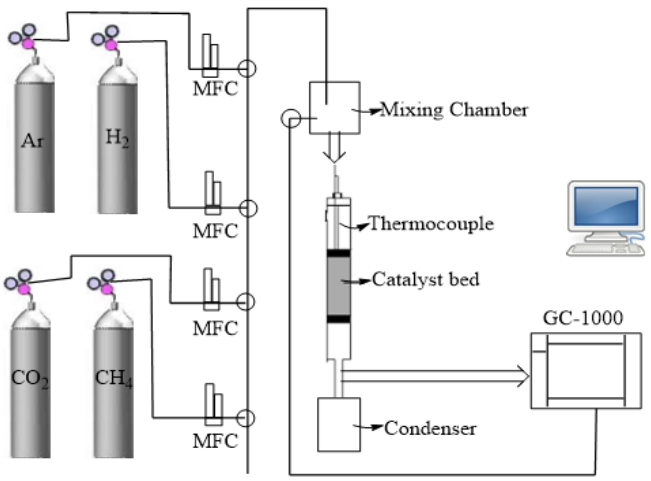

Fig. 1. Scheme of an automated flow-through installation [28].

2.3. Catalyst characterization

The morphology, crystallite dimensions, and habit of the phase components of the developed catalysts before and after catalytic reaction were studied by scanning electron microscopy (SEM) using JEOL JSM 65 10LV equipment with an electron acceleration tension of 20 kV and provided an energy dispersive X-ray (EDX) analyzer. The elemental content in the catalyst was determined by EDX spectra.

Phase identification and rate of crystallinity of the prepared catalysts before and after the catalytic reaction was conducted by the X-ray diffraction (XRD) using an HZG-4 (Germany) diffractometer equipped with a CuK_α radiation source (λ = 0.15406 nm) operating at 40 kV and 30 mA. The diffraction patterns were recorded at room temperature in the air with 2θ range from 20 to 80°. The crystallite domains will be determined by correlating the diffraction patterns with those in standard powder XRD files published by the International Center for Diffraction Data.

To determine the structure types (allotropies) of surface carbon deposited on the investigated catalysts before and after the DRM reaction, the same samples of the catalysts after the SEM-EDX study were moved into the analytical chamber of the Auger-electron spectrometer RIBER LAS-2000 (France) with the primary electron beam energy E_p = 5 keV. The surface was sectioned by sputtering of the analyzed surface (subsurfaces) through its bombardment by the argon ions with 2 keV energy and a sputtering rate ~10 Å/min that was provided at the selected ionic current density, and a series of layer-by-layer AES analyses were conducted.

Determination of the specific surface area of the catalysts was carried out by the method of low-temperature adsorption of nitrogen at -196 °C on an automatic BEL Japan Inc. The surface area is calculated using the BET equation.

Redox properties of the catalyst were studied by H_2 temperature-programmed reduction (H_2-TPR) on the USGA-101(Russia, Moscow). The sample (~0.050 g) was loaded in a quartz U-tube reactor. The samples were heated to 150 °C (at 10 °C /min) under Ar (purity 99.99%), to remove any surface species before analysis. After cooling to 50 °C, the sample was heated over a temperature range of 50–900 °C (at 10 °C/min) under 5% H_2 in Ar (at 30 ml/min).

3. Results

The effect of lanthanum oxide on the activity of Ni-Co/D in dry methane reforming at a reaction temperature of 800 °C is shown in Table.

The table shows that the introduction of lanthanum oxide into the composition of Ni-Co/D leads to an increase in its activity in the conversion of methane and carbon dioxide. The most promoting effect has lanthanum oxide at a content of 1.5 wt.%.

Increasing the content of lanthanum oxide above 1.5 leads to a decrease in the activity of the catalyst. This is in line with the observations of Gao et al. [29]. The decrease in catalyst activity with increasing La content is attributed by the authors to the fact that an excess of lanthanum not only loses the modification effect, but also increases the coverings over the catalyst. This leads to a decrease in catalytic activity, as well as specific surface area [30].

Ni-Co/D and Ni-Co-1.5La/D catalysts were selected for further research. The effect of reaction temperature on the activity of Ni-Co/D and Ni-Co-1.5La/D is shown in Fig. 2.

Since the reaction is highly endothermic, as the reaction temperature increased, the conversion of CH_4 and CO_2 on both catalysts increased. On the Ni-Co/D catalyst, the conversion of methane increased from 31 to 77.5%, carbon dioxide from 38 to 89%.

According to the literature [31–35], higher CO_2 conversion than CH_4 conversion can have several causes: the reverse water-gas shift reaction (RWGS), the reverse of Boudouard reaction, or a trapping effect of CO_2 by the basic sites of the surface.

The RWGS reaction (9) occurs in parallel with the DRM reaction (8), carbon dioxide interacts with hydrogen to form CO and H_2O [31, 32]. Water vapor can further participate in reactions 10 and 11 [33]. However, in our experiments, no water formation was observed at the reactor outlet.

The trapping effect of CO_2 by the basic sites of the surface can also contribute to the equilibrium shift towards higher values of carbon dioxide conversion. However, this effect will only be temporary until the adsorption capacity of the surface is reached [34].

Table

Effect of La_2O_3 concentration on Ni-Co/D activity

Sample	X_{CH4}	X_{CO2}	Y_{H2}	Y_{CO}	H_2/CO
Ni-Co/D	51	63	24	34	0.70
Ni-Co-1La/D	93	92	41	49	0.84
Ni-Co-1.5La/D	95	92	45	49	0.92
Ni-Co-2La/D	94	91	44	48	0.92

The reverse Boudouard reaction (12) also contributes to the consumption of CO_2, i.e., the interaction of carbon dioxide with surface carbon to form CO. The accumulation of carbon on the surface of catalysts during the DRM process at temperatures above 600 °C is mainly associated with the pyrolysis of methane (13). It should be noted that the carbon formed in this process is more reactive than the carbon formed in the Boudouard reaction, so it is easily oxidized in the presence of CO_2 to form CO.

The introduction of lanthanum oxide into the Ni-Co/D composition increases the activity of the catalyst, providing methane conversion close to that observed under thermodynamic equilibrium conditions in the temperature range of 700–850 °C. With an increase in the reaction temperature from 600 to 850 °C, the conversion of methane increases from 63 to 96%, and carbon dioxide from 48 to 92%. According to the results of TPR-H_2, BET, and SEM, the increase in catalyst activity with the introduction of lanthanum oxide is possibly associated with an increase in the dispersion of Ni-Co oxide phases and an increase in oxygen vacancy. In the studied temperature range, the conversion of methane is higher than that of CO_2, which may be due to the pyrolysis of methane with the formation of carbon and hydrogen (13). The presence of carbon on the surface of Ni-Co-1.5La/D was confirmed by the results of SEM and XRD (Fig. 6 c,d). According to [36], the pyrolysis of methane leads to an increase in the H_2/CO ratio above unity, which is not observed in our case. Apparently, the degree of conversion of CO_2 and CH_4, and the ratio of H_2/CO are affected by parallel reactions that can potentially occur in this system:

$$CO_2 + CH_4 \rightarrow 2CO + 2H_2 \quad (8)$$

$CO_2 + H_2 \rightarrow CO + H_2O$ – reverse water-gas shift reaction (RWGS) (9)

$$C + H_2O \rightarrow CO + H_2 \quad (10)$$

$CH_4 + H_2O \rightarrow CO + 3H_2$ – steam reforming of methane reaction (11)

$C + CO_2 \rightarrow 2CO$ – reverse Boudouard reaction (12)

$CH_4 \leftrightarrow C + 2H_2$ – pyrolysis of methane (13)

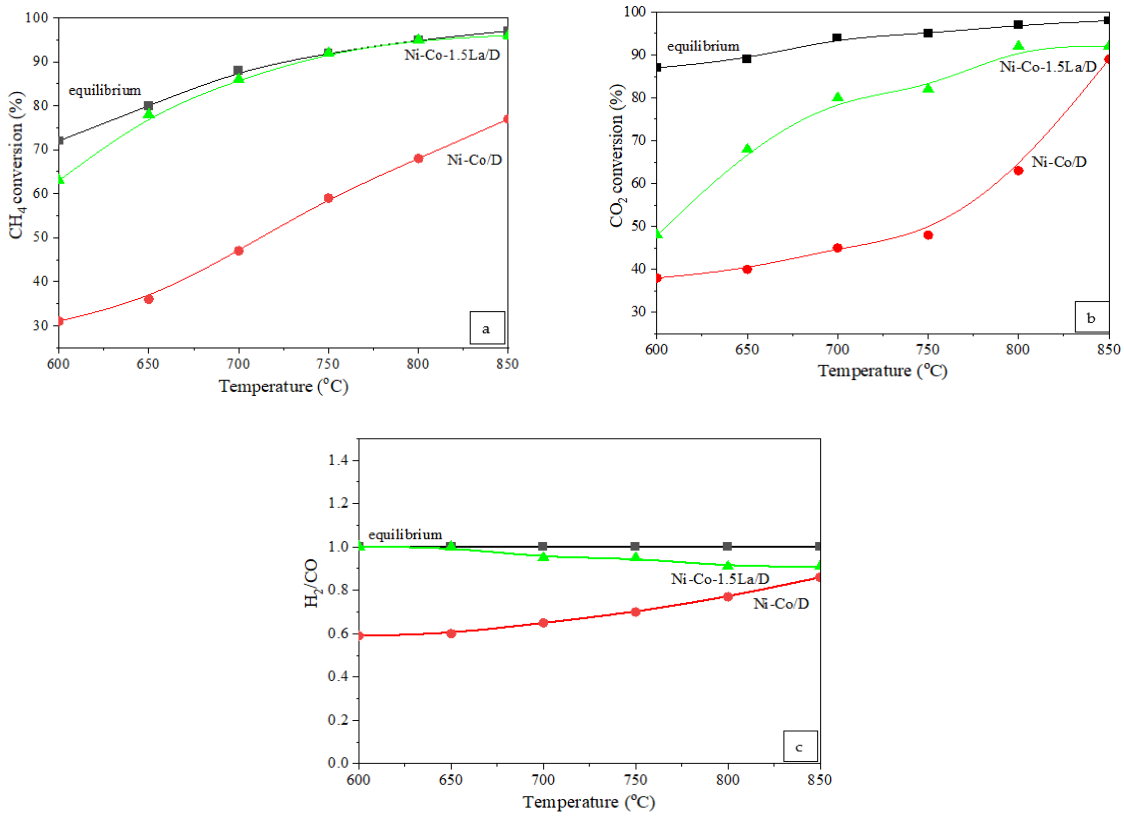

Fig. 2. Influence of reaction temperature in the range of 600–850 °C on the efficiency of catalysts: a) methane conversion; b) conversion of carbon dioxide; c) H_2/CO ratio.

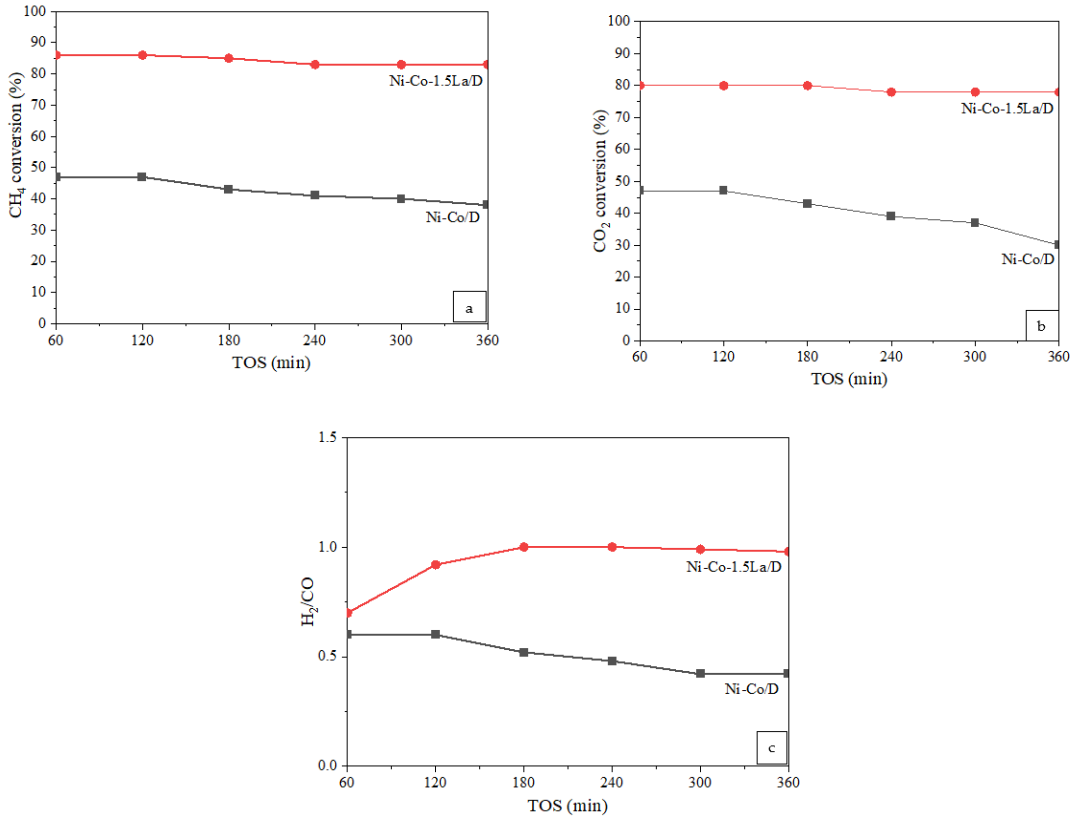

Fig. 3. Stability performance of catalysts in terms of CH_4 conversion (a), CO_2 conversion (b) and H_2/CO ratio (c) as a function of TOS at 700 °C.

The catalysts Ni-Co/D and Ni-Co-1.5La/D were tested at 700 °C for 6 h of continuous operation in dry methane reforming. The time-on-stream (TOS) conversions of the feedstock gases are plotted in Fig. 3.

The results show that for Ni-Co/D there is a significant deactivation, the deactivation coefficient for methane is 19%, and for carbon dioxide 36%.

Modification of Ni-Co/D with lanthanum oxide leads to an increase in the stability of the catalyst, the deactivation coefficient for methane is 3.4%, and for carbon dioxide 2.5%. This phenomenon may be associated with a better combination of methane decomposition and carbon dioxide activation, which prevents catalyst deactivation due to coke deposition and oxidation of the active metal [37].

The catalytic activity of oxide catalysts in redox reactions is usually explained by the oxygen-metal bond energy, the qualitative characteristics of which are the temperatures of the onset of the hydrogen consumption process, as well as the temperatures of the maxima in the TPR-H_2 curves. The TPR profiles of the catalysts are shown in Fig. 4.

For Ni/D, three peaks are observed with maxima T^1_{max} = 317 °C, T^2_{max} = 434 °C and T^3_{max} = 800 °C. According to the literature [38], the reduction of

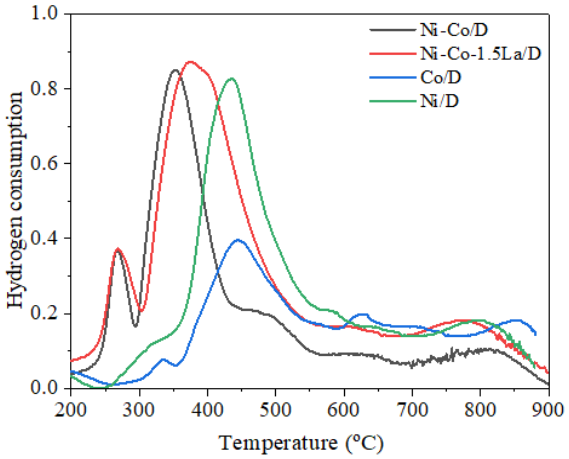

Fig. 4. TPR profiles of catalysts.

pure NiO consists of two reduction peaks corresponding to the stepwise reduction of nickel oxide: $NiO \rightarrow Ni^{\delta+} \rightarrow Ni^o$. The shoulder at T^1_{max} = 317 °C can be attributed to $NiO \rightarrow Ni^{\delta+}$ reduction and the intense peak at T^2_{max} = 434 °C to $Ni^{\delta+} \rightarrow Ni^o$ reduction. The high temperature peak at T^3_{max} = 800 °C may indicate a strong interaction between NiO and D, which may be caused by the formation of spinel (i.e. Ni-O-Al or Ni-O-Si). It is very difficult to attribute the peak to a particular phase, since the

natural support D has a complex composition and contains a microporous composition of silicon dioxide and aluminum oxide tetrahedra [39].

The Co/D sample showed complex recovery with various peaks in the range of 300–870 °C. It is known [40] that the reduction of Co_3O_4 is a two-stage process $Co_3O_4 \rightarrow CoO \rightarrow Co^0$, respectively, the observed peaks can be attributed to the reduction of Co_3O_4 crystallites of different sizes and different interactions with a support. The high temperature peak at 854 °C indicates the recovery of the Co-O-Al or Co-O-Si spinel structure [41].

Ni-Co/D and Ni-Co-1.5La/D catalysts have a complex reduction profile. For bioxide Ni-Co/D and polyoxide Ni-Co-1.5La/D catalysts, a new peak is observed at 267 °C. According to the literature [42], this low-temperature peak is associated with the formation of the nickel-cobalt compound $NiCo_2O_4$. The reduction of $NiCo_2O_4$ spinel was studied in [43], who, when analyzing the TPR of this compound in the temperature range of 27–727 °C, observed three reduction peaks (257, 315 ,and 367 °C), which were attributed to the gradual reduction of Ni^{2+}, Co^{3+} and Co^{2+} cations randomly distributed in the tetrahedral and octahedral positions of the spinel. According to the literature [43] peaks with a maximum at temperatures of 315 °C and 367 °C, correspond to the gradual reduction of $Co^{3+} \rightarrow Co^{2+}$ and $Co^{2+} \rightarrow Co^0$. The peak with a maximum of 257 °C was attributed by the authors to the reduction of Ni^{2+} cations.

Based on the literature, the low-temperature peak at T^1_{max} = 267 °C (Fig. 4.) can be associated with the reduction of Ni^{2+} cations in $NiCo_2O_4$. It is believed [44] that the electronic conductivity of nickel and cobalt compounds is higher than that of NiO or Co_3O_4 oxides themselves.

Peaks in the range of 300–550 °C may be associated with the overlap of the reduction peaks of both nickel and cobalt.

With the introduction of lanthanum oxide into the Ni-Co/D composition, the amount of hydrogen consumed to restore the peak at 267 °C increased, for Ni-Co/D it was A = 65 μmol/g, while for Ni-Co-1.5La/D it was 70 μmol/g. The addition of lanthanum oxide to the Ni-Co/D composition also leads to a shift in the temperature of the maximum to the high-temperature region (354→374 °C) and to an increase in the amount of hydrogen consumed for reduction from 426 to 576 μmol/g, which may indicate an increase in the dispersion of Ni-Co oxide phases and surface active oxygen [45–47].

It is known [47] that surface free oxygen (active oxygen) can effectively react with the CH_x groups formed during the reaction and, as a result, form CH_xO. Since CH_xO is considered to be a promising precursor for CO formation, its formation and degradation tend to strongly influence the catalytic activity in the DRM reaction.

In addition, the introduction of lanthanum leads to a decrease in the reduction temperature of the high-temperature peak from 821 to 776 °C, which is associated with the reduction of nickel or cobalt in spinel structures. A decrease in the reduction temperature indicates an increase in the dispersity of the particle size of nickel or cobalt in spinel structures [48].

At the same time, the amount of hydrogen consumed for reduction is 86 μmol/g for T = 776 °C and 55 μmol/g for T = 821 °C, which indicates an increase in the number of spinel structures. It is known [49, 50] that the reduction of $NiAl_2O_4$ spinel results in the formation of finely dispersed nickel (5–20 nm) stabilized in an Al_2O_3 matrix, which is highly active in the methane dissociation reaction. At high temperatures, spinel will be reduced to finely dispersed nickel by atomic hydrogen formed during the dissociation of methane. The amount of $NiAl_2O_4$ and its reducibility can not only affect the stability but also play an important role in the reactivity of catalysts. In other words, the more $NiAl_2O_4$ present in the nickel-containing catalysts, and the more easily it can be reduced, the better the catalyst will perform during DRM [51, 52].

The adsorption of carbon dioxide on Ni-Co/D and Ni-Co-1.5La/D catalysts at temperatures of 200, 300, 450, and 650 °C was studied, desorption was carried out at 750 °C. The obtained results (supplementary) showed that the introduction of lanthanum oxide (1.5 wt.%) into the composition of the Ni-Co/D leads to an increase in the amount of adsorbed carbon dioxide at all studied temperatures, which indicates an increase in centers for the adsorption of carbon dioxide.

Moreover, the addition of lanthanum leads to an increase in the specific surface area of the sample. The specific surface area of Ni-Co-1.5La/D is 40.9 m^2/g, while the specific surface area of Ni-Co/D is 26.7 m^2/g.

Figure 5 shows the SEM and EDX results of fresh samples of Ni-Co/D and Ni-Co-1.5La/D. Based on SEM images of both catalysts' samples (Fig. 5a and Fig. 5c) recorded before the DRM reaction, they look practically similar. No details of the structure of the catalysts deposited on the

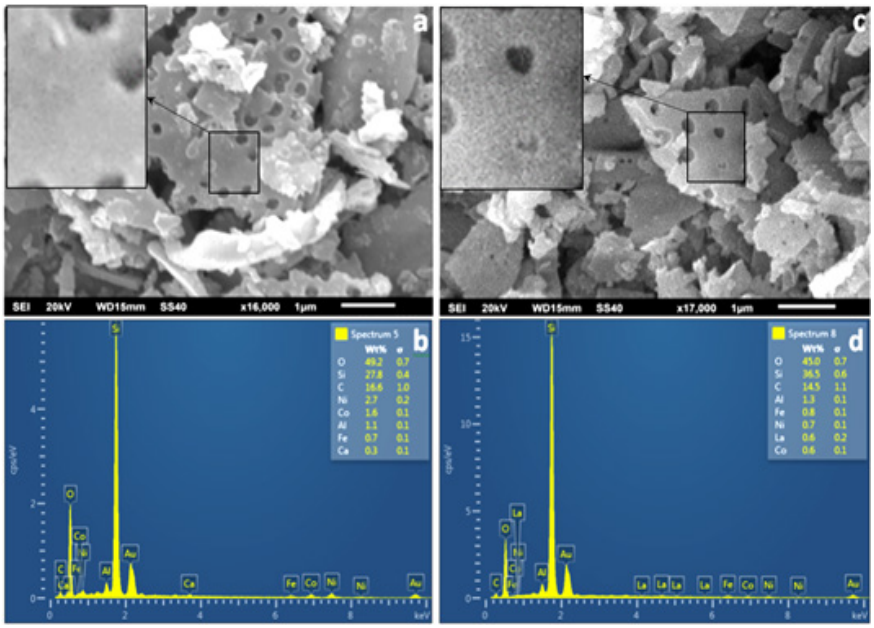

Fig. 5. SEM images and the respective EDX spectra of the surface of Ni-Co/D (a, b) and Ni-Co-1.5La/D catalysts (c, d) before the DRM reaction.

surfaces of the primary diatomite particles (the fractions of crashed frustules of diatomite with the characteristic cylindrical holes), constituting the support's granules, were observed within the resolution of the scanning microscope (~ 60 Å). Moreover, in addition to the EDX peaks of the catalysts (Ni and Co, Fig. 5b, and Ni, Co, and La, Fig. 5d), the peaks corresponding to the components of the diatomite support (Si, Al, Mg, Ca, Fe) also simultaneously present. Taking into account the depth of penetration of the accelerated electrons at 20 keV (<1 μ), generating secondary X-ray radiation, one may conclude that the thickness of the catalyst deposited on the surfaces of the diatomite particles in addition to the thickness of the sputtered conducting Au layer (~100 Å) and the thickness of the adsorbed from the atmosphere carbon (~50 Å) does not totally exceed a few hundreds of angstroms (≤1000 Å). In addition, a comparison of the SEM images corresponding to Ni-Co-1.5La catalyst deposits shows that the structure of Ni-Co catalyst deposit has a structure of a continuous thin film (see the magnified marked area in Fig. 5a) while the structure of Ni-Co-1.5La catalyst deposit is characterized by nano-grained uniform particles with the highly dispersive structure (see the magnified marked area in Fig. 5c). All these are in good correlation with the results of specific area measurements.

The presence of surface carbon in the amount of 14–16 wt.% is observed in the composition of fresh catalysts, which may have been formed during the heat treatment of catalysts at 300–500 °C in air.

In Figs. 6 and 7 the SEM/EDX, and XRD results obtained from the Ni-Co/D and Ni-Co-1.5La/D samples after their testing in the reaction are shown respectively. The SEM images of the surface of the Ni-Co/D catalyst sample after the reaction (Fig. 6a) demonstrate the formation of spherical nanoparticles of the reduced Ni with sizes from 200 to 1000 Å (see the magnified marked area in Fig. 6a).

These nanoparticles have a crystalline structure (111, 200, and 220 peaks corresponding to pure Ni crystal lattice are present in Fig. 7a, pattern – 2) formed during the sintering of the NiO catalyst's nano-clusters reduced by hydrogen. The latter is detected by a series of NiO peaks (111, 200, 220) on the XRD pattern taken before the reaction (Fig. 7a, pattern – 1).

Taking into consideration the low intensity of these peaks, the sizes of NiO crystallites (X-ray coherent scattering regions) are slightly bigger than the X-ray diffraction sensitivity threshold (≈ 100 Å). At the same time, the absence of the reflection peaks from the $NiCo_2O_4$, Co_3O_4 (or Co_2O_3) lattice in patterns 1 and 2, Fig. 7a, in addition to the series of peaks of NiO and the reduced Ni, confirms that cobalt oxide in the synthesized bioxide catalyst (Ni-Co) is available in the form of nanoparticles with the sizes much less than the X-ray diffraction sensitivity threshold (<100 Å). The presence of cobalt oxide in the catalyst is unambiguously detected in the samples in both conditions (before and after the DRM reaction), using the respective EDX spectra. The joint consideration of XRD and SEM/

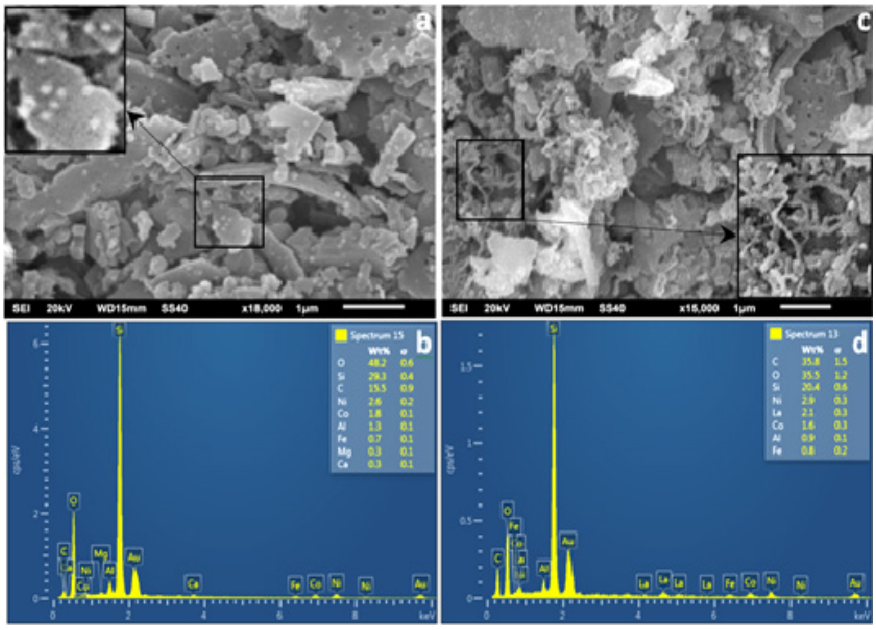

Fig. 6. SEM images and the respective EDX spectra of the surface of Ni-Co/D (a, b), and Ni-Co-1.5La/D (c, d) catalyst after the DRM reaction.

EDX data shows that in the process of DRM reaction on the surface of the (Ni-Co) catalyst synthesized on the granulated diatomite support, reduction of Ni and formation of spherical nanoparticles of pure Ni via sintering takes place. However, the highly dispersive oxide either is not reduced or if the reduction of Co takes place, it may appear in the form of the initial nanoparticles of cobalt oxide without sintering.

The analysis of SEM images of the catalyst system Ni-Co/D recorded after the DRM reaction shows that during the DRM reaction the formation of free carbon in the solid form of MWCNTs or CNWs does not take place on the given bioxide catalyst (Fig. 6a). Most likely, the formation of free carbon in a gaseous phase (reaction product) during the DRM reaction with the above catalyst is suppressed. The latter is witnessed by practically the same amount of surface carbon on the samples as before as well as after the reaction. The same was witnessed from practically the same intensity of (002) peaks of carbon (marked by "▼" at 2θ = 26.2˚) available in the X-ray diffractogram shown in Fig. 7a patterns – 1, and patterns – 2 respectively, recorded from the samples of the above bioxide catalyst system before and after the DRM reaction.

The consideration of the SEM-EDX data obtained from the samples of the catalyst Ni-Co-La/D after the DRM reaction shows that during the DRM reaction on the above polyoxide catalyst systems a formation of amorphous surface carbon and MWCNT simultaneously occurs (see the magnified marked area in Fig. 6c). It is well known [22] that the amorphous form of carbon is highly active. This type of carbon readily reacts with oxygen and is removed from the surface of the catalyst. The above phenomenon is also confirmed by the respective XRD patterns which show the increased intensity of the (002) peak of carbon (marked by "▼" at 2θ = 26.2˚) in addition to the series of peaks corresponding to Ni reduced by hydrogen from NiO in the polyoxide catalysts (Fig. 7b). Here should be noted that the absence of the respective peaks of pure Co and La in the diffractogram shown in Fig. 7b, patterns – 2, may be explained by the absence of the reduction process of the oxides of the above elements by hydrogen, or if reduction takes place, this process flows within the initial nanoparticles of the oxides of Co, La, without sintering of the reduced nanoparticles. The presence of diatomite in all the diffractograms (Fig. 7 a,b) was detected by the same variation of the background intensity and the superimposed broad diffraction peak around 2θ = 22˚, which can be attributed to the amorphous SiO_2, as the main component phase of diatomite.

In Fig. 8 a,b the series of peaks of carbon KLL differential AES spectra are shown which were obtained from the surfaces of the samples of the above catalyst systems in the 200–300 eV energy range after removing ~200 Å thickness anti-charging gold coating from the surfaces of the investigated samples via bombardment of the analyzed area with the argon ions of 2 keV energy.

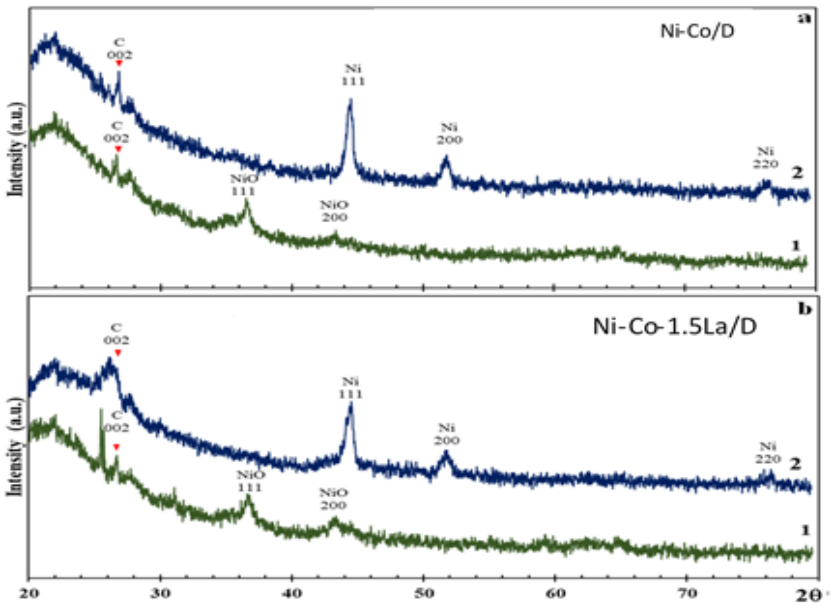

Fig. 7. Series of XRD patterns of samples Ni-Co/D (a) and Ni-Co-1.5La/D (b) recorded before (patterns – 1) and after (patterns – 2) the DRM reaction.

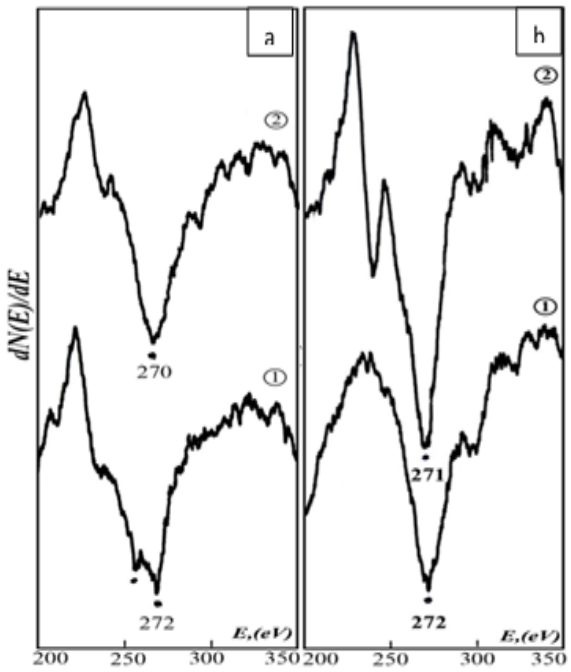

Fig. 8. The series of peaks of carbon KLL differential Auger-electron spectra recorded from the samples of Ni-Co/D (a) and Ni-Co-1.5La/D (b), recorded before (curves – 1) and after (curves – 2) the DRM reaction.

Consequently, the AES peaks (curves – 1) represent the state of the physical surface of the fresh catalyst systems before the deposition of gold coating, while the AES peaks presented in curves – 2 characterize the state of the surface composition of the spent catalyst systems' samples after the DRM reaction. The latter (Fig. 8 a,b) demonstrates the clearly expressed peculiarities of the fine structure (shape, energetic displacement of main and plasmon peaks, and their intensity ratio) of the first derivative of carbon atoms' KLL Auger-transition peaks, typical to the short-range order polyvariant configuration of carbon atoms' groups which can exist mostly in sp^2 hybridization on the Ni-Co/D catalyst, and mixed (sp^3 + sp^2) electronic hybridization on the Ni-Co-1.5La/D catalyst.

The absence of the peaks from the crystal lattices of the modifying components (Co_3O_4, La_2O_3) of the polyoxide catalysts in addition to the peaks of NiO (Fig. 7b), suggests that the modifying oxides in the synthesized polyoxide catalysts are presented in the form of nanoparticles with the sizes much smaller than the X-ray diffraction sensitivity threshold for the coherent scattering area size (<100 Å). The above phenomenon is also confirmed by the respective XRD patterns which show the increased intensity of the (002) peak of carbon (marked by "▼" at 2θ = 26.2˚) in addition to the series of peaks corresponding to Ni reduced by hydrogen from NiO in the polyoxide catalysts.

4. Conclusions

The bioxide (Ni-Co/D) and polyoxide (Ni-Co-1.5La/D) catalysts were successfully synthesized by capillary impregnation of granular diatomite. Those catalytic systems have been investigated before and after the DRM reaction tests in the temperature range of 600÷850 °C, using the mod-

ern SEM-EDX, XRD, AES, etc. methods. The introduction of 1.5 wt.% lanthanum oxide into the Ni–Co/D composition increases the activity of the catalyst, providing a methane conversion that is close under thermodynamic equilibrium conditions in the temperature range of 700–850 °C. With an increase in the reaction temperature from 600 to 850 °C, the conversion of methane increases from 63 to 96%, and carbon dioxide from 48 to 92%. In addition, the modification of Ni-Co/D with lanthanum oxide leads to an increase in the stability of the catalyst, the deactivation coefficient for methane is 3.4%, and for carbon dioxide 2.5%. While significant deactivation is observed for Ni-Co/D, the deactivation coefficient for methane is 19%, and for carbon dioxide 36%. According to the results of TPR-H_2, BET, and SEM, an increase in catalyst activity with the introduction of lanthanum oxide is possibly associated with an increase in the dispersion of Ni-Co oxide phases, and with an increase in surface active oxygen, which is involved in CO formation. In addition, an increase in the number of spinel structures contributed to the breaking of C–H bonds. The results show that the Ni-Co-1.5La polyoxide catalyst supported on natural diatomite has good DRM performance.

Acknowledgments

This work has been performed with the financial assistance of the International Science and Technology Center (ISTC) within project GE-2606.

References

[1]. C. He, S. Wu, L. Wang, J. Zhang, *J. Photochem. Photobiol.* 51 (2022) 100468. DOI: 10.1016/j.jphotochemrev.2021.100468

[2]. A. Ranjekar, G. Yadav, *J. Indian. Chem. Soc.* 98 (2021) 100002. DOI: 10.1016/j.jics.2021.100002

[3]. S. Wang, G. Lu, *Appl. Catal. A: Gen.* 169 (1998) 271280. DOI: 10.1016/S0926-860X(98)00017-9

[4]. K. Dossumov, G.E. Ergazieva, L.K. Myltykbaeva, M.M. Telbaeva, et al., *Theor. Exp. Chem.* 55 (2019) 137–142. DOI: 10.1007/s11237-019-09605-6

[5]. K. Sutthiumporn, S. Kawi, *Int. J. Hydrog. Energy* 36 (2011) 14435–14446. DOI: 10.1016/j.ijhydene.2011.08.022

[6]. B. Pholjaroen, N. Laosiripojana, P. Praserthdam, S. Assabumrungrat, *J. Ind. Eng. Chem.* 15 (2009) 488–497. DOI: 10.1016/j.jiec.2009.02.003

[7]. J. Xu, W. Zhou, J. Wang, Z. Li, et al., *Chinese J. Catal.* 30 (2009) 1076–1084. DOI: 10.1016/S1872-2067(08)60139-4

[8]. H.-S. Roh, K.-W. Jun, *Catal. Surv. Asia* 12 (2008) 239–252. DOI: 10.1007/s10563-008-9058-0

[9]. B. Adama, R. Ahmed, S. Shomefun, *Int. J. Chem. Eng.* 2 (2015) 46–52. https://journals.theired.org/journals/paper/details/6860.html

[10]. V. Sandoval-Bohórquez, E. Morales-Valencia, C. Castillo-Araiza, L. Ballesteros-Rueda, et al., *ACS Catal.* 11 (2021) 11478–11493. DOI: 10.1021/acscatal.1c02631

[11]. U. Guharoy, T.R. Reina, J. Liu, Q. Sun, et al., *J. CO2 Util.* 53 (2021) 101728. DOI: 10.1016/j.jcou.2021.101728

[12]. W.J. Jang, J.O. Shim, H.M. Kim, S.Y. Yoo, et al., *Catal. Today* 324 (2019) 15–26. DOI: 10.1016/j.cattod.2018.07.032

[13]. Y. Wang, L. Yao, S. Wang, D. Mao, et al., *Fuel Process. Technol.* 169 (2018) 199–206. DOI: 10.1016/j.fuproc.2017.10.007

[14]. N. Tran, Q. Le, N. Cuong, T. Nguyen, et al., *J. Energy Inst.* 93 (2020) 1571–1580. DOI: 10.1016/j.joei.2020.01.019

[15]. A. Movasati, S.M. Alavi, G. Mazloom, *Fuel* 236 (2019) 1254. DOI: 10.1016/j.fuel.2018.09.069

[16]. C. Jiang, E. Loisel, D.A. Cullen, J.A. Dorman, K.M. Dooley, *J. Catal.* 393 (2021) 215–229. DOI: 10.1016/j.jcat.2020.11.028

[17]. L. Baharudin, N. Rahmat, N.H. Othman, N. Shah, et al., *J. CO2 Util.* 61 (2022) 102050. DOI: 10.1016/j.jcou.2022.102050

[18]. Z. Bian, S. Das, M.H. Wai, P. Hongmanorom, et al., *ChemPhysChem* 18 (2017) 3117–3134. DOI: 10.1002/cphc.201700529

[19]. J. Zhang, H. Wang, A. Dalai, *J. Catal.* 249 (2007) 300–310. DOI: 10.1016/j.jcat.2007.05.004

[20]. L.K. Myltykbayeva, G.E. Ergazieva, M.M. Telbayeva, Z.R. Ismagilov, et al. *Eurasian Chem.-Technol. J.* 22 (2020) 187–195. DOI: 10.18321/ectj978

[21]. J. Wang, G. Zhang, G. Li, J. Liu, et al., *Int. J. Hydrog. Energy* 47 (2022) 7823–7835. DOI: 10.1016/j.ijhydene.2021.12.152

[22]. H. Wang, X. Dong, T. Zhao, H. Yu, et al., *Appl. Catal. B: Environ.* 245 (2019) 302–313. DOI: 10.1016/j.apcatb.2018.12.072

[23]. A. Tsoukalou, Q. Imtiaz, S. Kim, P. Abdala, et al., *J. Catal.* 343 (2016) 208–214. DOI: 10.1016/j.jcat.2016.03.018

[24]. G. Valderrama, A. Kiennemann, M. Goldwasser, *Catal. Today* 133 (2008) 142–148. DOI: 10.1016/j.cattod.2007.12.069

[25]. H.U. Hambali, A.A. Jalil, A.A. Abdulrasheed, T.J. Siang, et al., *Int. J. Hydrog. Energy* 47 (2022) 30759. DOI: 10.1016/j.ijhydene.2021.12.214

[26]. S. Khajeh Talkhoncheh, M. Haghighi, *J. Nat. Gas. Eng.* 23 (2015) 16–25. DOI: 10.1016/j.jngse.2015.01.020
[27]. K. Jabbour, N. El Hassan, A. Davidson, P. Massiani, et al., *J. Chem. Eng.* 264 (2015) 351–358. DOI: 10.1016/j.cej.2014.11.109
[28]. E. Kutelia, K. Dossumov, G. Yergaziyeva, D. Gventsadze, et al., *Adv. Mater. Lett.* 13 (2022) 22041709. DOI: 10.5185/amlett.2022.041709
[29]. X. Li, Q. Hu, Y. Yang, J. Chen, et al., *J. Rare Earths* 26 (2008) 864–868. DOI: 10.1016/S1002-0721(09)60022-3
[30]. L. Xiancai, L. Shuigen, Y. Yifeng, W. Min, et al., *Catal. Lett.* 118 (2007) 59–63. DOI: 10.1007/s10562-007-9140-7
[31]. M. Yusuf, M. Beg, M. Ubaidullah, S.F. Shaikh, et al., *Int. J. Hydrog. Energy* 47 (2021) 42150–42159. DOI: 10.1016/j.ijhydene.2021.08.021
[32]. B. Wang, X. Lu, S.T.B. Lundin, H. Kong, et al., *Energy Convers. Manag.* 268 (2022) 116050. DOI: 10.1016/j.enconman.2022.116050
[33]. A. Serrano-Lotina, L. Daza, *Int. J. Hydrog. Energy* 39 (2014) 4089. DOI: 10.1016/j.ijhydene.2013.05.135
[34]. C. Gennequin, M. Safariamin, S. Siffert, A. Aboukaïs, et al., *Catal. Today* 176 (2011) 139–143. DOI: 10.1016/j.cattod.2011.01.029
[35]. S.T. Phan, A.R. Sane, B.R. Vasconcelos, A. Nzihou, et al., *Appl. Catal. B: Environ.* 224 (2018) 310–321. DOI: 10.1016/j.apcatb.2017.10.063
[36]. S.N.A. Rosli, S.Z. Abidin, O.U. Osazuw, X. Fan, et al., *J. CO2 Util.* 63 (2022) 102109. DOI: 10.1016/j.jcou.2022.102109
[37]. C.Q. Pham, A.N.T. Cao, P.T.T. Phuong, L.K.H. Pham, et al., *J. Energy Inst.* 105 (2022) 314–322. DOI: 10.1016/j.joei.2022.10.004
[38]. W. Shan, M. Luo, P. Ying, W. Shen, et al., *Appl. Catal. A-Gen.* 246 (2003) 1–9. DOI: 10.1016/S0926-860X(02)00659-2
[39]. N. Dai, S. Yi, X. Zhang, L. Feng, et al., *Appl. Surf. Sci.* 607 (2023) 154886. DOI: 10.1016/j.apsusc.2022.154886
[40]. I. Luisetto, S. Tuti, E. Di Bartolomeo, *Int. J. Hydrog. Energy* 37 (2012) 15992–15999. DOI: 10.1016/j.ijhydene.2012.08.006
[41]. K. Dossumov, G.E. Ergazieva, B.T. Ermagambet, M.M. Telbayeva, et al., *Chem. Pap.* 74 (2020) 373–388. DOI: 10.1007/s11696-019-00921-8
[42]. M. Zhang, X. Sui, X. Zhang, M. Niu, et al., *Appl. Surf. Sci.* 600 (2022) 154040. DOI: 10.1016/j.apsusc.2022.154040
[43]. G. Cheng, Z. Cai, X. Song, X. Chen, et al., *Appl. Catal. B: Environ.* 304 (2022) 120988. DOI: 10.1016/j.apcatb.2021.120988
[44]. Y. Fang, X. Wang, Y. Chen, L. Dai, *J. Zhejiang Univ. Sci. A.* 21 (2020) 74–84. DOI: 10.1631/jzus.A1900535
[45]. S. Liang, T. Cai, J. Yuan, Q. Tong, et al., *J. Mol. Catal.* 533 (2022) 112762. DOI: 10.1016/j.mcat.2022.112762
[46]. K. Dosumov, G. Ergazieva, D. Churina, M. Tel'baeva, *Russ. J. Phys. Chem.* 88 (2014) 1806–1808. DOI: 10.1134/S0036024414100094
[47]. S. Gao, Y. Li, W. Guo, X. Ding, et al., *J. Mol. Catal.* 533 (2022) 112766. DOI: 10.1016/j.mcat.2022.112766
[48]. A.M. Haggar, A.E. Awadallah, A.A. Aboul-Enein, G.H. Sayed, *Mater. Chem. Phys.* 288 (2022) 126386. DOI: 10.1016/j.matchemphys.2022.126386
[49]. Y. Cesteros, P. Salagre, F. Medina, J.E. Sueiras, *Chem. Mater.* 12(2) (2000) 331–335. DOI: 10.1021/cm990154h
[50]. Y. Kwon, E. Eichler, B. Mullins, *J. CO2 Util.* 63 (2022) 102112. DOI: 10.1016/j.jcou.2022.102112
[51]. H. Qiu, J. Ran, X. Huang, Z. Ou, et al., *Int. J. Hydrog. Energy* 47 (2022) 34066–34074. DOI: 10.1016/j.ijhydene.2022.08.014
[52]. B.T. Dossumova, T.V. Shakiyeva, D. Muktaly, L.R. Sassykova, et al., *ChemEngineering* 6 (2022). DOI: 10.3390/chemengineering6050068